BIOCHEMISTRY
including biophysical chemistry & molecular biology

Article

pubs.acs.org/biochemistry

Correlations between the Electronic Properties of *Shewanella oneidensis* Cytochrome *c* Nitrite Reductase (ccNiR) and Its Structure: Effects of Heme Oxidation State and Active Site Ligation

Natalia Stein,[†,∥] Daniel Love,[†] Evan T. Judd,[‡] Sean J. Elliott,[‡] Brian Bennett,[§,∥] and A. Andrew Pacheco*[,†]

[†]Department of Chemistry and Biochemistry, University of Wisconsin—Milwaukee, Milwaukee, Wisconsin 53211, United States

[‡]Department of Chemistry & Molecular Biology, Cell Biology and Biochemistry Program, Boston University, 590 Commonwealth Avenue, Boston, Massachusetts 02215, United States

[§]Department of Biophysics, Medical College of Wisconsin, Milwaukee, Wisconsin 53226, United States

Supporting Information

ABSTRACT: The electrochemical properties of *Shewanella oneidensis* cytochrome *c* nitrite reductase (ccNiR), a homodimer that contains five hemes per protomer, were investigated by UV−visible and electron paramagnetic resonance (EPR) spectropotentiometries. Global analysis of the UV−vis spectropotentiometric results yielded highly reproducible values for the heme midpoint potentials. These midpoint potential values were then assigned to specific hemes in each protomer (as defined in previous X-ray diffraction studies) by comparing the EPR and UV−vis spectropotentiometric results, taking advantage of the high sensitivity of EPR spectra to the structural microenvironment of paramagnetic centers. Addition of the strong-field ligand cyanide led to a 70 mV positive shift of the active site's midpoint potential, as the cyanide bound to the initially five-coordinate high-spin heme and triggered a high-spin to low-spin transition. With cyanide present, three of the remaining hemes gave rise to distinctive and readily assignable EPR spectral changes upon reduction, while a fourth was EPR-silent. At high applied potentials, interpretation of the EPR spectra in the absence of cyanide was complicated by a magnetic interaction that appears to involve three of five hemes in each protomer. At lower applied potentials, the spectra recorded in the presence and absence of cyanide were similar, which aided global assignment of the signals. The midpoint potential of the EPR-silent heme could be assigned by default, but the assignment was also confirmed by UV−vis spectropotentiometric analysis of the H268M mutant of ccNiR, in which one of the EPR-silent heme's histidine axial ligands was replaced with a methionine.

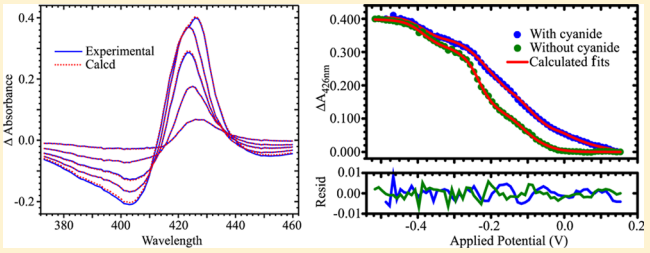

Cytochrome *c* nitrite reductase (ccNiR) is a soluble periplasmic bacterial enzyme that catalyzes the six-electron reduction of nitrite to ammonia[1] and can also catalyze reduction of NO or hydroxylamine to ammonia.[2,3] The active protein is a homodimer, which depending on the organism from which it is obtained, has protomeric molecular masses ranging from 52 to 65 kDa.[4−10] In all homologues studied so far, each protomer contains five *c*-type hemes; four are six-coordinate, bis-histidine ligated, and low-spin, and the fifth is five-coordinate and high-spin, and unique among *c*-hemes in having a lysine residue in the proximal axial position (Figure 1). The hemes in ccNiR are closely packed, with iron−iron distances of <13 Å, which facilitates rapid inter-heme electron transfer. Thus, the six-coordinate hemes appear to act as electron shuttles that efficiently carry electrons from the enzyme's external physiological electron donor to the five-coordinate active site where nitrite reduction occurs.[4−10]

Ammonifying bacteria use ccNiR to reduce the terminal electron acceptor nitrite in anaerobic respiration,[1,11,12] and this appears to be the enzyme's primary role. However, there is also some evidence that ccNiR has a role in mitigating oxidative and nitrosative stress, not just in response to nitrite, but also to NO, hydroxylamine, and even hydrogen peroxide.[2,6,13,14] This hypothesis has been reinforced by the isolation of a ccNiR ortholog and a related nitrite-reducing multiheme protein from bacteria that are incapable of dissimilatory nitrite reduction.[6,14]

Many aspects of the heme arrangement within ccNiR are replicated in other proteins,[15,16] and how a common structural motif is optimized for specialized roles is a subject of much investigation. For example, comparative mechanistic studies of ccNiR and *Nitrosomonas europaea* hydroxylamine dehydrogenase (HDH[a]), a multiheme enzyme that catalyzes the oxidation of hydroxylamine to nitrite in ammonia-oxidizing bacteria,[11,12] have been conducted to understand how ccNiR and HDH have been evolutionarily optimized to catalyze similar reactions in opposite directions.[10,17−19] Ultimately, meaningful interpretation of mechanistic data for ccNiR and HDH requires that the redox properties of the enzymes under reaction conditions of a

Received: March 27, 2015
Revised: June 2, 2015
Published: June 4, 2015

DOI: 10.1021/acs.biochem.5b00330
Biochemistry 2015, 54, 3749−3758

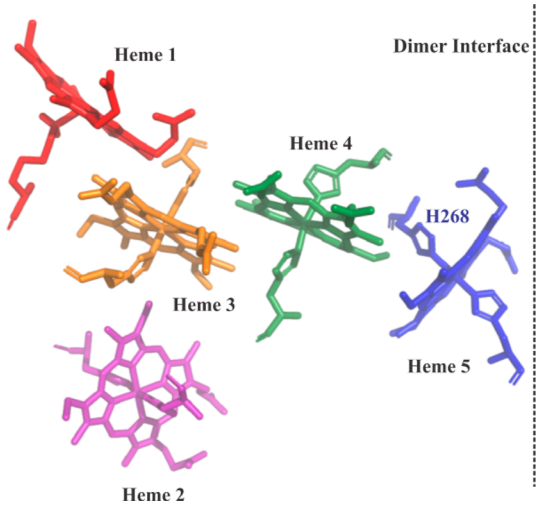

Figure 1. Five hemes from one of the ccNiR protomers and their axial ligands, with axial ligand His 268 that was subjected to mutagenesis identified. The dashed vertical line represents a dimer interface for the complete dimer. The hemes are color-coded to match spectral assignments made in the text and Table 2.

given study be thoroughly understood. This article presents UV−vis and EPR spectropotentiometric studies of wild-type ccNiR from *Shewanella oneidensis* in the presence and absence of the strong-field ligand cyanide, and a UV−vis spectropotentiometric analysis of the H268M ccNiR mutant (Figure 1). CcNiR's physiological substrate N-bound nitrite is a strong-field ligand, and the major objective of these studies was to determine the effect of such ligands on the enzyme's midpoint potentials. In addition to addressing this question, the combined studies led to the assignment of all of *S. oneidensis* ccNiR's heme midpoint potentials.

MATERIALS AND METHODS

General Materials. Potassium cyanide, sodium nitrite, ethylenediaminetetraacetic acid disodium salt (EDTA), anthroquinone-2-sulfonic acid sodium salt monohydrate, methyl viologen hydrate, and safranine O were purchased from Acros Organics. Anthroquinone-1,5-disulfonic acid disodium salt hydrate, hexaammineruthenium(III) chloride, potassium indigo trisulfonate, potassium indigo tetrasulfonate, and indigo carmine were purchased from Sigma-Aldrich. Sodium chloride and 2-[4-(2-hydroxyethyl)piperazin-1-yl]ethanesulfonic acid (HEPES) sodium salt were from Fisher Scientific. The mediator Diquat [6,7-dihydrodipyrido[1,2-*a*:2′,1′-*c*]-pyrazinediium dibromide (Table 1)] was synthesized using the method described by Homer and Tomlinson.[20]

Protein Purification and Handling. Wild-type *S. oneidensis* ccNiR ($ccNiR_{wt}$) was purified from a high-yield expression system and stored in aliquots at −80 °C, as described previously.[10]

To ensure that the H268M mutant of ccNiR ($ccNiR_{H268M}$) could be readily separated from the constitutively expressed wild-type enzyme, *S. oneidensis* TSP-C was transformed with a TEV cleavable 10-histidine tag (C-terminal) in PHSG298.[21] The H268M mutation was then introduced using an Agilent QuikChange Lightning site-directed mutagenesis kit with the primers 5′GAGACCTGGAAGATGGGCATCATGGGTAAA-AATAACGTCTCGTGT3′ and 5′ACACGAGACGTTATTT-TTACCCATGATGCCCATCTTCCAGGTCTC3′. The mutation was verified by sequencing. Transformed cells were grown in 1 L batches of LB medium at 30 °C for 24 h, after which $ccNiR_{H268M}$ was purified using a Ni-6-Sepharose column (GE Healthcare), and the His tag was removed by overnight digestion with recombinant TEV protease, as described previously.[22]

Table 1. Mediators Used for Spectropotentiometry

mediator	ε° (V vs SHE)	used for	concentration (μM)
phenazine methosulfate	0.08	UV−vis	25
gallocyanin	−0.020	EPR	25
hexaammineruthenium(III) chloride	−0.020	UV−vis	100
indigo tetrasulfonate	−0.030	EPR	25
indigo trisulfonate	−0.080	EPR	25
indigo carmine	−0.125	UV−vis, EPR	25
anthraquinone 1,5-disulfonic acid	−0.175	UV−vis, EPR	25
anthraquinone 2-sulfonic acid	−0.255	UV−vis, EPR	25
safranine O	−0.289	UV−vis, EPR	25
Diquat[a]	−0.390	UV−vis, EPR	25
methyl viologen	−0.449	UV−vis, EPR	25

[a] Diquat: 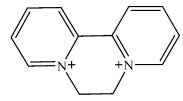

UV−Vis Spectropotentiometric Titrations of ccNiR. UV−vis spectropotentiometry experiments were performed using a BASi Epsilon EC potentiostat to set the potential, and a CARY Bio 50 UV−vis spectrophotometer to record the spectra at each applied potential. The complete apparatus was housed in an anaerobic glovebox. Controlled potentiometric electrolysis of the solution was performed in an optically transparent thin-layer electrode cell similar to the one used in earlier work by this group,[10] and elsewhere.[23,24] A solution of ccNiR (25−30 μM dimer) and redox mediators (Table 1) was prepared in 50 mM HEPES and 200 mM NaCl (pH 7.0). UV−vis spectra in the range of 250−800 nm were collected at 10 mV intervals between +50 and −600 mV (vs SHE). A Ag/AgCl electrode (BASi, model RE-5B) was used as a reference. Cyclic voltammograms of methyl viologen were collected before and after collection of the data sets, and the calculated midpoint potential (ε°_m = −0.449 V[25]) was used to account for any drift in the reference electrode. Spectra recorded with the mediator solutions in the absence of ccNiR were subtracted from the corresponding ccNiR data sets to account for any spectral changes caused by the mediators during the titration. The corrected data sets were analyzed using programs written within the commercially available software package Mathcad 15 (PTC Software). Data analysis broadly followed the methodology used previously by this group;[10] details specific to this work are provided in the Results and the Supporting Information.

Electron Paramagnetic Resonance (EPR) Titrations of ccNiR. EPR spectra were recorded on an EleXsys E600 spectrometer (Bruker), equipped with an ER4122SHQ resonator, an Oxford Instruments ITC503 temperature controller, and an ESR900 helium flow cryostat (Oxford

DOI: 10.1021/acs.biochem.5b00330
Biochemistry 2015, 54, 3749−3758

Instruments). A microwave frequency of 9.386 GHz was employed; precise frequencies were recorded for each spectrum by a built-in microwave counter. Background signals were recorded on a frozen water sample and subtracted in Xepr (Bruker Biospin) with small-field corrections for slight frequency differences. Magnetic-field modulation and phase-sensitive detection at 100 kHz were employed, with a 5 G (0.5 mT) field modulation amplitude; other recording parameters (time constant and conversion time) were chosen such that the resolution was limited by the modulation amplitude. A microwave power of 1 mW and a temperature of 10 K were employed. At a higher power (e.g., 5 mW), rapid passage effects were clearly evident in the spectra, whereas at a lower power or higher temperatures, the spectra were either unacceptably noisy or certain features were relaxation-broadened beyond detection. The combination of 1 mW at 10 K with the high-Q resonator thus provided the best compromise. Typical ccNiR concentrations for the experiments were 25−30 μM in dimer. For EPR−spectropotentiometric titrations, the samples were prepared using a bulk electrolysis cell with platinum mesh as the working electrode. In a typical experiment, 4 mL of a ccNiR solution was added to the bulk electrolysis cell. The sample was stirred rapidly, and the desired potential was applied. Upon stabilization, a 250 μL subsample was removed from the cell and transferred into an EPR tube. The EPR tube was then placed into a test tube, which was stoppered with a butyl rubber stopper, removed from the glovebox, and immediately submerged in liquid nitrogen. Samples were subsequently stored at −80 °C and kept on dry ice during transportation (<8 h).

RESULTS

Effect of Cyanide on the Electrochemical Properties of ccNiR. Figure 2 shows selected UV−visible spectral changes observed with a decrease in the potential applied to a solution initially containing 23.3 μM fully oxidized ccNiR dimer and 75 μM cyanide. Singular-value decomposition (SVD) analysis[26,27] showed that five components contribute to the spectral changes. The data were well-fit using a model in which each protomer of the ccNiR dimer is successively reduced in one-electron increments, as shown in Scheme 1 and eqs 1 and 2, whose complete derivation can be found in ref 10. Equations 1a−1c are derived from the Nernst equation in exponential form and correlate the concentration of each partially reduced species $C_{red(m)}$ with the applied potential, ε_{app}. In the equations, ε°_{m} is the midpoint potential associated with one-electron reduction of the $(m-1)$th reduced species and C_T is the total ccNiR concentration in solution. For the data of Figure 2, the best fit was obtained by setting n, the number of electrons transferred in each reduction event, to 1. Equation 2 is a matrix form of Beer's law in which $\mathbf{C_{red}}$ is a matrix of concentrations wherein each column corresponds to a unique reduced species $C_{red(m)}$ and each row to a specific applied potential, $\mathbf{\Delta\varepsilon}$ is an extinction coefficient difference matrix in which each column corresponds to a unique reduced species and each row to a wavelength, $\mathbf{\Delta A}$ is the SVD-processed absorbance difference matrix in which each column contains a spectrum at a fixed applied potential and each row shows how absorbance varies with potential at a fixed wavelength, and l is a scalar representing the path length of the OTTLE cell. The procedure by which Figure 2 data were fit with eqs 1 and 2 was analogous to one described previously,[10] and the calculated least-squares best fits are overlaid on the experimental data in the figure. The

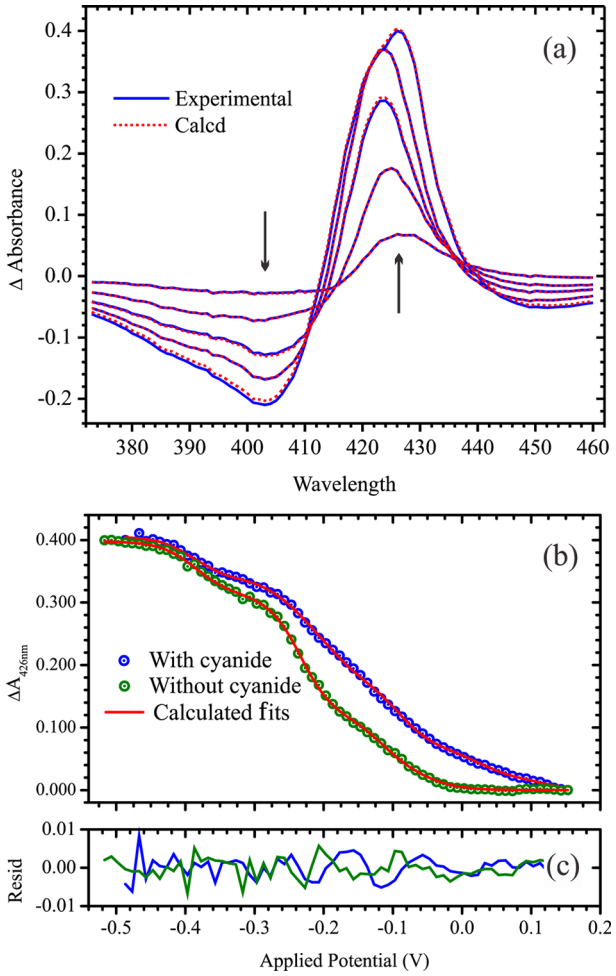

Figure 2. (a) UV−vis spectral changes obtained upon exposing a solution initially containing 23.3 μM fully oxidized ccNiR dimer and 75 μM cyanide to applied potentials of −27, −137, −217, −317, and −487 mV vs SHE; arrows indicate the direction of change. Solid blue lines show the experimentally obtained data, whereas the dashed red lines were calculated from least-squares fitting to five Nernstian potentials (Scheme 1 and eqs 1 and 2), as described in ref 10. (b) Blue circles show the absorbance difference vs applied potential slice taken at 426 nm from the spectra of panel a; green circles show an equivalent slice obtained from a global fit of the spectral changes accompanying potentiometric reduction of a 23.3 μM solution of ccNiR dimer in the absence of cyanide (spectral changes are provided as Supporting Information). In both cases, the solid red traces are the least-squares best fits obtained from a global analysis of the data. (c) Residuals for panel b.

fitting procedure yielded extinction coefficient difference spectra for ccNiR species C_{red1}−C_{red5} at varying stages of reduction (Figure 3a), and the concentrations of the partially reduced species as a function of applied potential (Figure 3b).

The model embodied in Scheme 1 and eqs 1 and 2 is consistent with the fact that each ccNiR protomer contains five structurally distinct hemes. However, it is important to emphasize that each species $C_{red(m)}$ reflects only the number of electrons that have been added to the protomer as a whole. In some cases, each added electron may end up localized on a specific heme, but the model also allows for the possibility that it will delocalize among several hemes, as has been proposed previously and is discussed further below.[10]

DOI: 10.1021/acs.biochem.5b00330
Biochemistry 2015, 54, 3749−3758

Scheme 1. Definitions of the Species Used in Equations 1 and 2[a]

$$Ox + e^- \longrightarrow C_{red1}$$
$$C_{red1} + e^- \longrightarrow C_{red2}$$
$$C_{red2} + e^- \longrightarrow C_{red3}$$
$$C_{red3} + e^- \longrightarrow C_{red4}$$
$$C_{red4} + e^- \longrightarrow C_{red5}$$

$$C_{red(m)} = \frac{C_T \prod_{m=1}^{5} E_m}{denom} \quad \text{Eq. 1a}$$

where:

$$denom = 1 + E_1\{1 + E_2[1 + E_3[1 + E_4(1 + E_5)]]\} \quad \text{Eq. 1b}$$

$$E_m = \exp\left[\frac{nF}{RT}(\varepsilon_m^0 - \varepsilon_{app})\right] \quad \text{Eq. 1c}$$

$$\Delta\varepsilon = \Delta A \cdot [C_{red}(C_{red}^T C_{red})^{-1}] \cdot \frac{1}{l} \quad \text{Eq. 2}$$

[a]Ox refers to fully oxidized ccNiR, as isolated from the purification process. C_{red1}–C_{red5} refer to the one-electron-reduced to five-electron-reduced species, respectively.

The most striking difference observed between data collected in the presence and absence of cyanide is a 70 mV positive shift in the first midpoint potential when cyanide is present. This is seen graphically in Figure 2b, and also in Table 2, which compare data collected in the presence and absence of cyanide using the same apparatus: the first ccNiR midpoint potential is seen to shift from −44 to +27 mV versus SHE in the presence of cyanide. Some variability in the calculated midpoint potentials accompanies changes in apparatus (ref 10), but in all cases, the characteristic shift to a higher potential was observed. Differences in the midpoint potentials associated with the remaining reduction events were much less pronounced (Table 2), from which we conclude that C_{red1} in Scheme 1 corresponds to reduction of the active site heme, and that binding of cyanide to this site effects the shift to a higher potential.

The spectropotentiometric titrations of ccNiR in the presence and absence of added cyanide were repeated using EPR spectroscopy in place of UV–vis. EPR spectra are highly sensitive to the hemes' structural microenvironment, allowing one to readily correlate observed spectral changes to changes at specific hemes.

Figure 4 shows the EPR spectral changes observed when a 25 μM solution of fully oxidized ccNiR dimer was exposed to 100 μM cyanide. Addition of the cyanide extinguished a component of the spectrum that is characterized by a derivative-shaped signal with a trough at $g' = 2.87$, and another characterized by EPR absorption extending from zero field to $g' \approx 10$.[b] The latter signal was enhanced in parallel mode [$B_0 \| B_1$ (not shown)] and is characteristic of an integer-spin system. These features were previously assigned to the high-spin ($S = {}^5/_2$) Fe(III) active site, weakly exchange-coupled to one of the low-spin ($S = {}^1/_2$) hemes,[17] and are similar to those assigned previously to the active site of *Escherichia coli* ccNiR.[7] The heme closest to the active site heme 1 is heme 3, and in the past, it has been assumed that heme 3 and heme 1 are weakly exchange-coupled;[7,17] however, the situation may be more complex, for reasons presented below. The disappearance of the $g' = 2.87$ and $g' > 10$ signals upon addition of cyanide suggests that the strong-field ligand has bound to the active site and caused a high-spin to low-spin transition, consistent with the UV–vis spectropotentiometric results reported above.

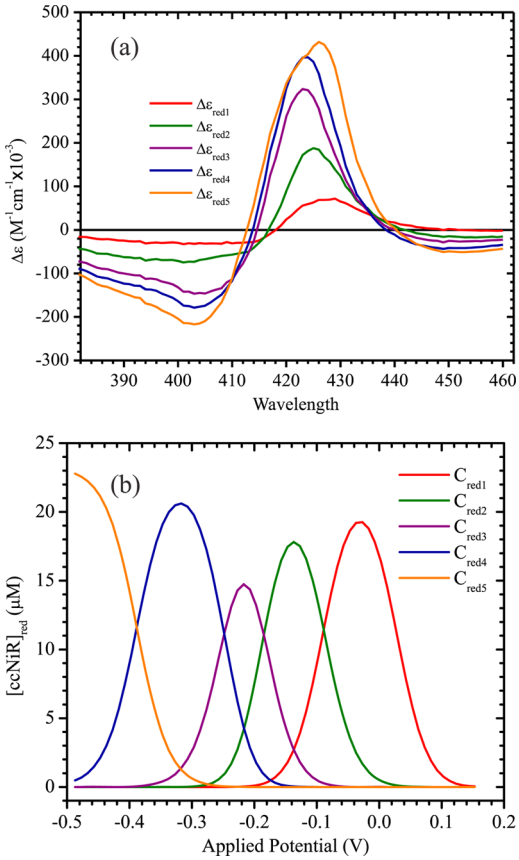

Figure 3. (a) Extinction coefficient difference spectra corresponding to each of the reduced ccNiR species C_{red1}–C_{red5} (Scheme 1), as calculated using eqs 1 and 2 by the procedure described in ref 10, for the data obtained in the presence of cyanide (Figure 2a). (b) Calculated concentrations of C_{red1}–C_{red5} as a function of the applied potential (vs SHE) for the same data. In panels a and b, the traces are color-coded to match the hemes in Figure 1 to which they are tentatively assigned (see the text for details). Note that the values of C_{red1}–C_{red5} are given in terms of dimer concentrations, but those of $\boldsymbol{\Delta\varepsilon}$ are given in terms of the protomer concentrations, to allow direct comparison with earlier reports where this was done (for example, in refs 10 and 17). The amplitudes for the $\boldsymbol{\Delta\varepsilon}$ spectra corresponding to the ccNiR dimer will be twice those shown in panel a.

The remaining signals in spectra in Figure 4 can be assigned to low-spin Fe(III) hemes in a variety of environments, by comparison with well-established literature precedents. Three $g_x = 2.94$, $g_y = 2.29$, and $g_z = 1.52$ features are characteristic of low-spin ferric hemes with imidazoles that are parallel to each other on opposite sides of the heme plane, an arrangement that gives rise to rhombic EPR spectra.[7,29] CcNiR has two such hemes in each protomer: hemes 2 and 3 in Figure 1, either of which could give rise to a rhombic trio. Notice, however, that the signals are present in the presence and absence of cyanide; though the $g_x = 2.94$ feature is mostly hidden by the more intense $g = 2.87$ trough when cyanide is absent, the $g_y = 2.29$ and $g_z = 1.52$ features are clearly visible in both spectra of Figure 4. Thus, if in the absence of cyanide hemes 1 and 3 are weakly exchange-coupled as proposed above and in the literature,[7,17] and give rise to the unique set of signals with $g' = 2.87$ and $g' > 10$, then the rhombic signal set must be due to heme 2 alone.

DOI: 10.1021/acs.biochem.5b00330
Biochemistry 2015, 54, 3749–3758

Table 2. Midpoint Potentials of *S. oneidensis* ccNiR Hemes (in volts vs the standard hydrogen electrode) for Wild-Type ccNiR ($ccNiR_{wt}$) in the Presence and Absence of Cyanide and for the H268M Mutant ($ccNiR_{H268M}$)[b]

	$ccNiR_{wt}$[a]	$ccNiR_{wt}$ + CN^-	$ccNiR_{H268M}$
$\mathcal{E}^0_1$	−0.0440±002 (H1)	0.027 (H1)	0.060 (H5)
$\mathcal{E}^0_2$	−0.110±0.004 (H4)	−0.089 (H4)	−0.035 (H1)
$\mathcal{E}^0_3$	−0.21±0.02 (H2)	−0.185 (H2)	−0.116 (H4)
$\mathcal{E}^0_4$	−0.257±0.017 (H5)	−0.248 (H5)	−0.209 (H2)
$\mathcal{E}^0_5$	−0.382±0.004 (H3)	−0.388 (H3)	−0.338 (H3)

[a]Average of two experiments performed using the same apparatus, but different ccNiR batches. Experiments conducted using different spectroelectrochemical apparatus, or different techniques, exhibited greater variability in the midpoint potential values obtained (ref 10). [b]Colors and labels H1−H5 suggest possible assignments to the hemes in Figure 1; see the text for details.

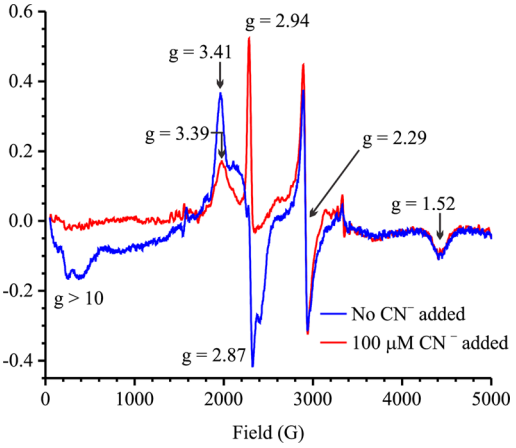

Figure 4. X-Band EPR spectrum for a 25 μM solution of fully oxidized ccNiR dimer (blue trace) and same except that the solution also contained 100 μM cyanide (red trace).

A final weak feature, seen at g = 3.39 in the presence of cyanide, is characteristic of hemes that are in highly axial environments, to the point where the d_{xz} and d_{yz} orbitals are virtually degenerate and the unpaired electron can be considered to be shared between them. Often termed "highly axial low-spin" (HALS) signals,[29−31] these signals are difficult to resolve, and usually, only the $g \sim 3-4$ signal is detected. HALS-type signals can arise from low-spin ferric hemes with imidazoles perpendicular to each other on opposite sides of the heme plane,[7,29] and/or from hemes with the plane of the axial imidazole(s) *meso* with respect to the heme nitrogens (i.e., bisecting the N−Fe−N right angle[32]). In addition, HALS-type signals have also been observed for low-spin ferric heme cyanide model compounds.[33] The *S. oneidensis* ccNiR crystal structure reveals two hemes with imidazoles roughly perpendicular [hemes 4 and 5 (Figure 1)]. Therefore, the g = 3.39 feature seen in the presence of cyanide could be due to one or more of ccNiR hemes 4 and 5, and/or the cyanide-bound active site; the spectropotentiometric titration described next allows these possibilities to be distinguished. Note that a feature at almost the same position (g = 3.41) is also seen in the absence of cyanide but is significantly more intense than the g = 3.39 feature seen in its presence. One or more HALS signal-generating hemes almost certainly contribute to this feature, but it seems probable that the weakly exchange-coupled hemes 1 and 3 also contribute, making the signal stronger than it typically is.

Figure 5 shows the EPR spectral changes observed with a decrease in the potential applied to the solution initially

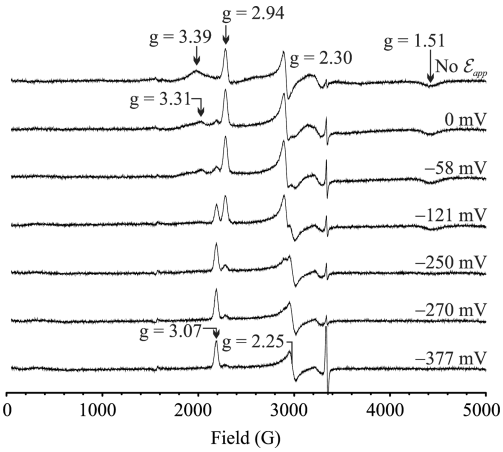

Figure 5. X-Band EPR spectra obtained for a solution initially containing 25 μM fully oxidized ccNiR dimer and 100 μM cyanide, upon exposing it to the applied potentials shown (vs SHE). An additional signal that grows in at g = 1.31 as the applied potential is decreased can be viewed in an expanded spectrum provided as Supporting Information.

containing 25 μM fully oxidized ccNiR dimer and 100 μM cyanide, in addition to the mediators from Table 1. At an applied potential of 0 mV versus SHE, the most notable change is a decrease in the intensity, and a shift to a slightly higher field, of the g = 3.39 HALS signal. This change is attributed to reduction of the active site heme, on the basis of the UV−vis spectropotentiometric results of Figure 2b above that show the cyanide-bound active site being reduced with a midpoint potential of +20 mV. The fact that the putative HALS signal does not completely disappear as the active site is reduced confirms that it is actually a composite of at least two overlapping signals, one arising from the active site and the second from heme 4 or 5 or both, each of which has mutually perpendicular imidazoles on opposite sides of the heme plane (Figure 1).[7,29]

As the potential is decreased further from 0 to −377 mV, a second rhombic signal set with g_x = 3.07, g_y = 2.25, and g_z = 1.31 appears, while the residual HALS signal, now with maximal intensity at g = 3.31, disappears concomitantly. In addition, the original rhombic signal set with g_x = 2.94, g_y = 2.30, and g_z = 1.51 also gradually fades, though its disappearance lags behind the appearance of the new rhombic set. As stated above, in ccNiR rhombic signal sets would be expected for magnetically isolated ferric hemes 2 and 3, on the basis of their axial ligand geometry.[7,29] Because the initial g_x = 2.94, g_y = 2.30, and g_z = 1.51 set was assigned to heme 2 above and in previous reports,[7,17] the new rhombic set must arise from heme 3.

The fact that the new rhombic set for heme 3 appears as the second HALS signal disappears can be explained if the residual

DOI: 10.1021/acs.biochem.5b00330
Biochemistry 2015, 54, 3749−3758

HALS signal arises from a pair of magnetically coupled ferric hemes rather than from a single heme. In this scenario, ferriheme 3 would generate a rhombic signal set and the adjacent ferriheme 4 a HALS signal, if magnetically isolated, but in practice, they couple to generate a HALS-like signal. Then, if the normally HALS-generating heme 4 is reduced first, the remaining now-uncoupled but still-oxidized heme 3 will display its typical rhombic signals. Via correlation of the UV−vis and EPR results, the midpoint potential of heme 4 is thus assigned as −89 mV, the second reduction event listed in Table 2. In the UV−vis spectropotentiometric results, the midpoint potential for the third reduction event is −185 mV, which is assigned to heme 2 because during EPR the disappearance of the heme 2 signal set somewhat lags behind the appearance of the heme 3 set.

The rhombic signal set attributed to heme 3 is still present at −377 mV, at which only a single heme [with a midpoint potential of −388 mV (Table 2)] remains partially oxidized according to the UV−vis results. Heme 3 is thus seen to be the last one reduced with a midpoint potential of −388 mV. By default, the midpoint potential of −248 mV (Table 2) is then assigned to heme 5. The HALS signal expected for this heme was not detectable; however, a site-directed mutagenesis experiment (described below) provides additional support for the assignment of the −248 mV midpoint potential to heme 5. The color coding of the midpoint potentials listed in Table 2 summarizes their plausible assignments to the hemes in Figure 1, on the basis of the UV−vis and EPR spectropotentiometric results.

At low applied potentials, the EPR spectral changes that accompany a decrease in potential in the absence of cyanide (Figure 6) are similar to those seen in its presence (Figure 5).

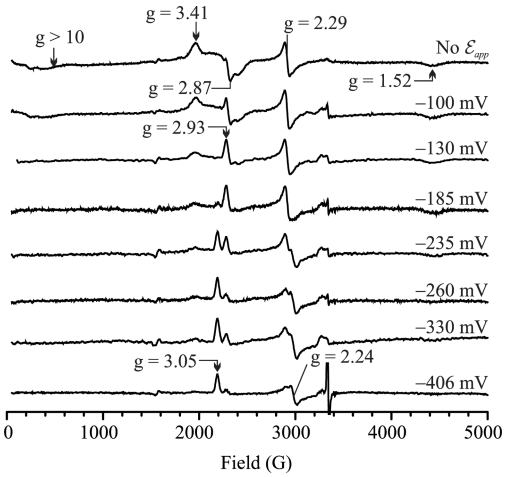

Figure 6. X-Band EPR spectra obtained for a solution initially containing 25 μM fully oxidized ccNiR dimer in the absence of cyanide, upon its exposure to the applied potentials shown (vs SHE). An additional signal that grows in at g = 1.31 as the applied potential is decreased can be viewed in an expanded spectrum provided as Supporting Information.

The similarity extends to the appearance of a new rhombic signal set at g_x = 3.05, g_y = 2.24, and g_z = 1.31 and concomitant disappearance of a HALS signal at $g \sim 3.3$−3.4 as the potential drops below approximately −150 mV, consistent with magnetic coupling between ferric hemes 3 and 4, which disappears when heme 4 is reduced. At higher potentials, the changes observed in the absence of cyanide are different because the ferric active site starts out as high-spin and is coupled to at least one nearby low-spin heme (Figures 4−6). Previously, the active site's characteristic signals at g' = 2.87 and g' > 10 were attributed to weak exchange coupling with one low-spin heme, presumably heme 3, which is closest (Figure 1; see above and refs 7 and 17). However, given that ferric heme 3 appears to be coupled to ferric heme 4, it now looks like the characteristic active site signals may actually arise from a more complex three-way magnetic interaction among the active site (heme 1), heme 3, and heme 4.

UV−Vis Spectropotentiometry of the H268M *S. oneidensis* ccNiR Mutant. In ccNiR, His268 is one of the axial ligands for heme 5 in each protomer (Figure 1). Figure 7 shows selected UV−vis spectral changes observed upon decreasing the potential applied to a solution initially containing 19.9 μM oxidized ccNiR$_{H268M}$ dimer. An analysis similar to that described above for the wild type in the presence of cyanide (fully described in the Supporting Information) yielded the fits shown by the dashed red traces in Figure 7, midpoint potentials for five discrete reduction steps of the mutant protein (Table 2), and extinction coefficient difference spectra corresponding to the five partially reduced species (Supporting Information).

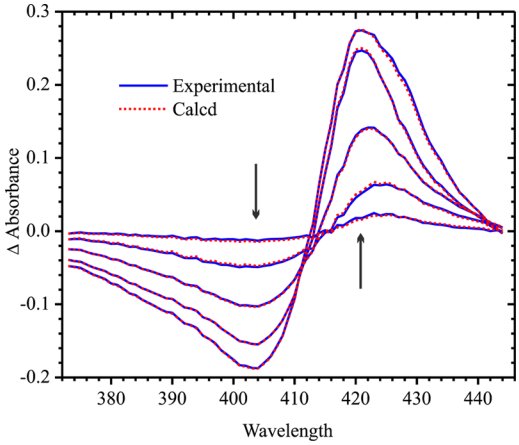

Figure 7. UV−vis spectral changes obtained upon exposing a solution initially containing 19.9 μM fully oxidized ccNiR$_{H268M}$ dimer to applied potentials of 0, −100, −180, −270, and −500 mV vs SHE; arrows indicate the direction of change. Solid blue lines show the experimentally obtained data, whereas the dashed red lines were calculated from least-squares fitting to four Nernstian potentials, as described in the Supporting Information.

As indicated by the color coding of the midpoint potentials in Table 2, ε°_2−ε°_5 for ccNiR$_{H268M}$ most closely match ε°_1−ε°_3 and ε^0_5 for ccNiR$_{wt}$; ccNiR$_{H268M}$ shows no midpoint potential that closely corresponds to ε°_4 of ccNiR$_{wt}$. Similarly, ccNiR$_{wt}$ exhibits no midpoint potential that corresponds to the high potential ε°_1 of ccNiR$_{H268M}$. Thus, it appears that the H268M mutation causes the ε°_4 of ccNiR$_{wt}$ to shift dramatically to the positive, becoming ε°_1 in ccNiR$_{H268M}$. This provides strong evidence that ε°_4 of ccNiR$_{wt}$ corresponds to heme 5, whose axial ligand was mutated in ccNiR$_{H268M}$.

Note that the shapes of the ccNiR$_{H268M}$ spectra at low potentials (Figure 7) are notably different from those of the wild type at low potentials (as seen, for example, in Figure 2a). This can also be seen more conveniently in Figure S6 of the Supporting Information, which compares the extinction

DOI: 10.1021/acs.biochem.5b00330
Biochemistry 2015, 54, 3749−3758

coefficient difference spectra for the reduced species C_{red1}−C_{red5} obtained from the UV−vis spectropotentiometric titrations of $ccNiR_{H268M}$ and $ccNiR_{wt}$. For the wild type, the extinction coefficient difference spectra for C_{red4} and C_{red5} exhibit noticeable red shifts in the signals that have maximal amplitudes above 420 nm. This shift is completely absent in the spectrum of $\Delta\varepsilon_{red4}$ of $ccNiR_{H268M}$ but appears as a shoulder in that of $\Delta\varepsilon_{red5}$ (Figure S6 of the Supporting Information). Again, this is consistent with assignment of $\Delta\varepsilon_{red4}$ to reduction of heme 5 in $ccNiR_{wt}$, but not in $ccNiR_{H268M}$.

DISCUSSION

By combination of results of UV−vis and EPR spectropotentiometric titrations, specific midpoint potentials have been assigned to each of the five hemes per protomer of *S. oneidensis* $ccNiR_{wt}$ in the presence and absence of the strong-field ligand cyanide, and of the $ccNiR_{H268M}$ variant in the absence of cyanide (Table 2). The UV−vis spectropotentiometric apparatus used herein yielded highly reproducible midpoint potential values. This allowed the midpoint potential of the active site heme to be identified as the only one that shifted significantly in the presence of cyanide, and that of heme 5 as the only one to shift notably upon mutation of one of its axial ligands to a methionine in the $ccNiR_{H268M}$ variant.

Apart from heme 5, reduction of each of the remaining hemes could be associated with distinct EPR spectral changes. At some applied potentials, two or more of the ferrihemes appear to be involved in complex magnetic interactions that resisted attempts at simulation and cannot be directly interpreted solely on the basis of literature precedent. Despite this, we can be reasonably confident about the midpoint potential assignments because at key points during the EPR spectropotentiometric titration, the highly characteristic rhombic signals of uncoupled ferrihemes 2 and 3 are detectable and can be tracked.[7,29] In this regard, the *S. oneidensis* ccNiR behavior is similar to that of *N. europaea* HDH, a homotrimer that contains eight hemes per protomer. In HDH, two pairs of ferrihemes in each protomer are magnetically coupled at high potentials and uncouple as one heme in each pair is reduced.[34] In the case of HDH, unambiguous simulation of the coupling necessitated a multifrequency EPR study, which tracked how the signals from the coupled hemes shifted with frequency; similar studies are planned for ccNiR in the future. Pereira et al. also reported seeing signals appear in the EPR spectrum of the *Desulfovibrio vulgaris* ccNiR as hemes uncoupled during reduction,[6] though in that case spectral interpretation was complicated by the fact that the *D. vulgaris* enzyme is isolated as a complex with the tetraheme NrfH, which adds four extra hemes to the mix.

The analysis presented thus far assumes that each reduction event identified in the UV−vis spectropotentiometric titrations has 1:1 correspondence with reduction of a unique heme. However, for *S. oneidensis* ccNiR in the absence of cyanide, we previously suggested that each of the first two one-electron reduction events of Scheme 1 might actually spread the electron density among two or more hemes.[10] Reduction of high-spin ferrihemes typically yields UV−vis difference spectra with maximal positive deflection above 430 nm. A distinct peak at 430 nm was observed for *E. coli* ccNiR,[35] but not for the *S. oneidensis* enzyme in the absence of cyanide (Figure S1 of the Supporting Information and ref 10). The *S. oneidensis* spectra could be explained if the first and second reduction events distributed the electron density between the high-spin active site and one or more of the low-spin hemes, because the latter invariably exhibit maxima below 430 nm in the UV−vis region.[10] Of note, evidence of this type of behavior was observed in a theoretical analysis of HDH reduction.[36] Given the complexity of the EPR spectra associated with zero- to three-electron-reduced ccNiR in the absence of cyanide, the possibility of delocalized one-electron reduction steps still cannot be ruled out by the study presented here (nor can it be ruled out for the $ccNiR_{H268M}$ variant). In the presence of cyanide, the EPR spectral changes associated with $\varepsilon^{\circ}{}_1$ and $\varepsilon^{\circ}{}_2$ are much more discrete, a fact that is aided by the large shift to positive potential of $\varepsilon^{\circ}{}_1$. Under these conditions, the assignment of $\varepsilon^{\circ}{}_1$ and $\varepsilon^{\circ}{}_2$ to reduction of specific hemes is more robustly supported.

In addition to the spectropotentiometric studies of *S. oneidensis* ccNiR reported here and in a previous study,[10] some of the *E. coli* ccNiR heme midpoint potentials were similarly assigned in two earlier studies, using a combination of magnetic circular dichroism[35] and EPR[7] spectropotentiometries. Though the spectropotentiometric behaviors for the *S. oneidensis* and *E. coli* ccNiRs are similar superficially, closer inspection reveals some striking differences between the two enzymes.

The biggest difference observed between the *S. oneidensis* and *E. coli* ccNiR spectropotentiometric profiles is seen in the midpoint potential of heme 2 (Figure 1), which is substantially higher in *E. coli* ccNiR than it is in the *S. oneidensis* enzyme [−37 mV (ref 7) vs −214 mV (Table 2) in the absence of strong-field ligands]. The *E. coli* and *S. oneidensis* enzymes are structurally very similar, but the region in which they differ most significantly is on the protein surface near heme 2.[10] This region appears to be the physiological entry point for electrons,[7,9] and the structural difference is believed to reflect the fact that *E. coli* and *S. oneidensis* ccNiR use different physiological electron donors, with *E. coli* using NrfB and *S. oneidensis* using CymA.[10] Visual inspection of the *E. coli* and *S. oneidensis* ccNiR structures in space-filling mode (Figure 8) reveals that the propionate group of heme 2 is neutralized by hydrogen bonding with Arg201 in the *E. coli* structure, whereas it is solvent-exposed in the *S. oneidensis* ccNiR. Propionate neutralization has been shown to provoke significant positive shifts in heme midpoint potentials[37] and thus could account for the difference observed here. The heme edge in the *S. oneidensis* ccNiR also appears to be somewhat more solvent-exposed than that in the *E. coli* enzyme (Figure 8); a decrease in the level of solvent exposure is likewise known to shift heme midpoint potentials in the positive direction.[38]

For *E. coli* ccNiR, both MCD and EPR clearly show that the active site [heme 1 (Figure 1)] is the second heme reduced, after heme 2, with a midpoint potential of −107 mV.[7,35] By contrast, in the *S. oneidensis* enzyme, the active site is reduced first, with a midpoint potential of −44 mV in the absence of strong-field ligands, and one of +20 mV in the presence of cyanide (Table 2). Interestingly, an early EPR spectropotentiometric titration of the *D. vulgaris* ccNiR suggested that the active site of this enzyme was one of the last hemes to be reduced, with a midpoint potential of approximately −210 mV.[6]

Detection of the heme 3 signals for *S. oneidensis* ccNiR greatly simplified the unambiguous assignment of the EPR spectra for this enzyme. These signals are still visible at the lowest potential monitored (−377 and −406 mV in Figures 5 and 6, respectively), showing that heme 3 is the last one reduced (see Results). In the case of *E. coli* ccNiR, the trio of

DOI: 10.1021/acs.biochem.5b00330
Biochemistry 2015, 54, 3749−3758

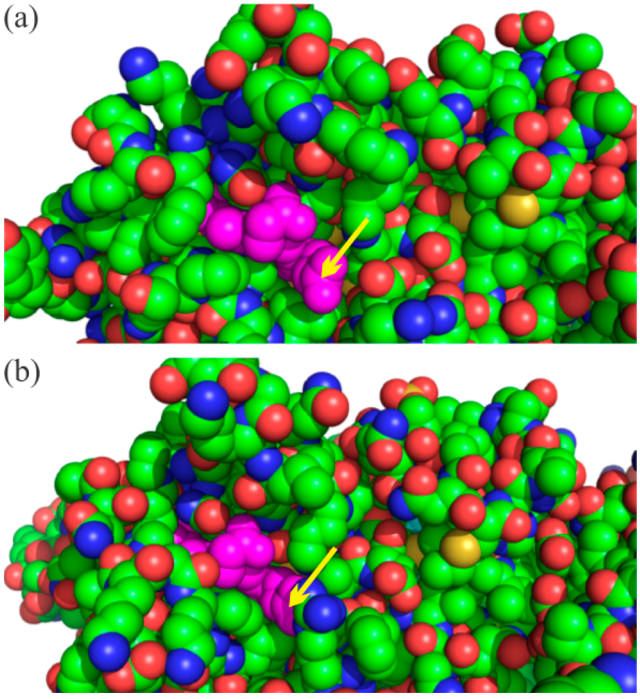

Figure 8. Space-filling view of the ccNiR surface in the vicinity of heme 2 (purple) for (a) the *S. oneidensis* enzyme and (b) the *E. coli* enzyme. The yellow arrows point to the heme propionate that is solvent-exposed in the *S. oneidensis* enzyme but hydrogen-bonded to Arg201 in the *E. coli* enzyme.

rhombic signals expected for heme 3 was not detected at any applied potential, which to date has made it impossible to unambiguously assign any low-spin hemes other than heme 2.[7,35] As for *S. oneidensis* ccNiR, only one HALS signal was clearly detectable in the *E. coli* enzyme, and this was associated with a reduction event centered at a midpoint potential of −292 mV.[7,35] Such a value most closely corresponds to that of the *S. oneidensis* enzyme's heme 5 midpoint potential, though as seen above one cannot assume that hemes from the two enzymes will exhibit comparable potentiometric behavior, despite their structural similarity.

It is perhaps instructive to rationalize some aspects about the order of heme reduction for *S. oneidensis* ccNiR on the basis of the following simple Coulombic argument. First, when electrons are added to hemes 1, 2, and 4, the reduced hemes are separated from each other by oxidized hemes 3 and 5 (Figure 1). This arrangement will lead to weaker Coulombic repulsions between reduced hemes than any permutation in which three electrons are added to each protomer to reduce either heme 3 or heme 5; such permutations all force electrons to go on adjacent hemes. Once three electrons have been added to each protomer, the fourth electron will have to go to either heme 3 or heme 5. Both options will put reduced hemes in direct contact with each other. However, heme 3 sits at the branch point among hemes 1, 2, and 4 within one protomer and so will be surrounded by three reduced hemes, whereas heme 5 will be surrounded by two: heme 4 from the same protomer and heme 5 from the adjacent one (Figure 1). Clearly, an electron added to heme 5 would experience less repulsion, so one would predict this heme to be reduced before heme 3, which is observed experimentally. A similar pattern in the order of heme reduction was observed for HDH,[36,39] which as mentioned before shares many similarities with ccNiR in regard to heme arrangement.[10,40] In the case of HDH, the Coulombic rationale was supported by a computational study.[36] Note also that this rationale does not contradict anything that has been confirmed so far for the order of heme reduction in *E. coli* ccNiR: hemes 1 and 2 are among the first reduced, even if in an order different from that seen for the *S. oneidensis* enzyme, and heme 5 may be among the last reduced.[7,35]

Importantly, the observed difference in order of heme reduction between the *S. oneidensis* and *E. coli* ccNiRs suggests that a specific order is not critical to ccNiR function, because the two enzymes exhibit virtually identical specific activities.[10] This might seem surprising, but one should bear in mind that differences in midpoint potentials measured experimentally in a protein with multiple redox-active sites are typically much larger than the differences felt by a single electron moving from site to site in an otherwise fully oxidized protein. The latter differences, which are likely to be small in ccNiR, are more physiologically relevant. The reason for the aforementioned phenomenon is that it is impossible to measure the midpoint potential of a low potential redox-active site until one has reduced the higher-potential sites in the same protein, and each additional electron added to the protein will decrease the midpoint potentials of the remaining sites because of strengthened Coulombic repulsion.[36] An extraordinary example of this is observed for the midpoint potentials of HDH.[34,36,39] The midpoint potentials of the eight HDH hemes from each protomer were resolved using spectropotentiometry and found to span a dramatically wide range of 700 mV, from +288 to −412 mV.[34,39] However, in a computational study in which a single electron was moved from heme to heme in fully oxidized HDH, the heme midpoint potentials spanned a range of only 417 mV, from +264 to −153 mV.[36] The 417 mV difference reflects the effects of the local environment on the individual HDH hemes, while the additional ∼300 mV difference observed in the spectropotentiometric titrations arises because the lower-potential hemes are reduced after the higher-potential ones, and their midpoint potentials are affected by these prior reductions. In the case of ccNiR, most of the dramatic difference in heme 2's midpoint potential value between the *E. coli* and *S. oneidensis* enzymes probably arises from the fact that this heme is reduced after hemes 1 and 4 in *S. oneidensis* but is the first to be reduced in *E. coli*.

Probably the most important result from this study is the fact that the strong-field ligand cyanide causes such a large positive shift in the active site's midpoint potential. Nitrite, the physiological substrate for ccNiR, is also a strong-field ligand when N-bound and might be expected to provoke a similar shift in midpoint potential.[3] We have now verified this conjecture in a series of experiments that provided important new insights into the mechanism of ccNiR-catalyzed nitrite reduction. These experiments will be presented in an upcoming article.

■ ASSOCIATED CONTENT

Supporting Information

Spectral changes and calculated intermediate concentrations via spectropotentiometric titration of ccNiR in the absence of cyanide, expanded EPR spectrum of ccNiR during spectropotentiometric titration, and analysis of the UV−vis spectropotentiometric titration of $ccNiR_{H268M}$. The Supporting Information is available free of charge on the ACS Publications website at DOI: 10.1021/acs.biochem.5b00330.

DOI: 10.1021/acs.biochem.5b00330
Biochemistry 2015, 54, 3749−3758

AUTHOR INFORMATION

Corresponding Author

*E-mail: apacheco@uwm.edu. Phone: (414) 229-4413. Fax: (414) 229-5530.

Present Address

[‖]N.S. and B.B.: Physics Department, Marquette University, P.O. Box 1881, Milwaukee, WI 53201.

Funding

Supported by National Science Foundation Grants MCB-1121770 and MCB-1330809. D.L. gratefully acknowledges support from the University of Wisconsin—Milwaukee's Office of Undergraduate Research.

Notes

The authors declare no competing financial interest.

ABBREVIATIONS

ccNiR, cytochrome *c* nitrite reductase; HDH, hydroxylamine:ferricytochrome *c* oxidoreductase; UV−vis, ultraviolet−visible; EPR, electron paramagnetic resonance; SHE, standard hydrogen electrode; EDTA, ethylenediaminetetraacetic acid disodium salt; HEPES, 2-[4-(2-hydroxyethyl)piperazin-1-yl]-ethanesulfonic acid sodium salt; Diquat, 6,7-dihydrodipyrido-[1,2-*a*:2′,1′-*c*]pyrazinediium dibromide; SVD, singular-value decomposition; HALS, highly axial low-spin.

ADDITIONAL NOTES

[a]In the past, this enzyme has been more commonly termed hydroxylamine oxidase (or oxidoreductase), abbreviated as HAO. However, the currently accepted name for the enzyme (EC 1.7.2.6) is hydroxylamine dehydrogenase, while its correct systematic name is hydroxylamine:ferricytochrome *c* oxidoreductase.

[b]The quantity g', or g' value, is used to denote the effective g value of a resonance in the EPR spectrum that is not necessarily determined by the Landé g factor, whereas g, or g value, implies the Landé g factor. In the case of high-spin systems (with $S > {}^1/_2$), the g' value is often largely a function of the zero-field splitting constant, D. For $S = {}^5/_2$ and $g = 2$, the usual case for high-spin Fe(III), $g' \leq 10$; if $g' > 10$, then either $S > {}^5/_2$, if noninteger, or S has an integer value (see ref 28).

REFERENCES

(1) Simon, J. (2002) Enzymology and bioenergetics of respiratory nitrite ammonification. *FEMS Microbiol. Rev. 26*, 285−309.

(2) Poock, S., Leach, E., Moir, J., Cole, J., and Richardson, D. (2002) Respiratory Detoxification of Nitric Oxide by the Cytochrome *c* Nitrite Reductase of *Escherichia coli*. *J. Biol. Chem. 277*, 23664−23669.

(3) Einsle, O., Messerschmidt, A., Huber, R., Kroneck, P. M. H., and Neese, F. (2002) Mechanism of the six-electron reduction of nitrite to ammonia by cytochrome c nitrite reductase. *J. Am. Chem. Soc. 124*, 11737−11745.

(4) Einsle, O., Messerschmidt, A., Stach, P., Bourenkov, G. P., Bartunik, H. D., Huber, R., and Kroneck, P. M. H. (1999) Structure of cytochrome c nitrite reductase. *Nature 400*, 476−480.

(5) Einsle, O., Stach, P., Messerschmidt, A., Simon, J., Kroger, A., Huber, R., and Kroneck, P. M. H. (2000) Cytochrome c nitrite reductase from *Wolinella succinogenes*: Structure at 1.6 angstrom resolution, inhibitor binding, and heme-packing motifs. *J. Biol. Chem. 275*, 39608−39616.

(6) Pereira, I., LeGall, J., Xavier, A., and Teixeira, M. (2000) Characterization of a heme *c* nitrite reductase from a non-ammonifying microorganism, *Desulfovibrio vulgaris* Hildenborough. *Biochim. Biophys. Acta 1481*, 119−130.

(7) Bamford, V. A., Angove, H. C., Seward, H. E., Thomson, A. J., Cole, J. A., Butt, J. N., Hemmings, A. M., and Richardson, D. J. (2002) Structure and spectroscopy of the periplasmic cytochrome c nitrite reductase from *Escherichia coli*. *Biochemistry 41*, 2921−2931.

(8) Cunha, C. A., Macieira, S., Dias, J. M., Almeida, G., Goncalves, L. L., Costa, C., Lampreia, J., Huber, R., Moura, J. J. G., Moura, I., and Romao, M. J. (2003) Cytochrome c nitrite reductase from *Desulfovibrio desulfuricans* ATCC 27774: The relevance of the two calcium sites in the structure of the catalytic subunit (NrfA). *J. Biol. Chem. 278*, 17455−17465.

(9) Rodrigues, M., Oliveira, T., Pereira, I., and Archer, M. (2006) X-ray structure of the membrane-bound cytochrome *c* quinol dehydrogenase NrfH reveals novel haem coordination. *EMBO J. 25*, 5951−5960.

(10) Youngblut, M., Judd, E. T., Srajer, V., Sayyed, B., Goelzer, T., Elliott, S. J., Schmidt, M., and Pacheco, A. A. (2012) Laue crystal structure of *Shewanella oneidensis* cytochrome *c* nitrite reductase from a high-yield expression system. *JBIC, J. Biol. Inorg. Chem. 17*, 647−662.

(11) Ehrlich, H. L. (2002) *Geomicrobiology*, 4th ed., Marcel Dekker, Inc., New York.

(12) Fenchel, T., King, G. M., and Blackburn, T. H. (1998) *Bacterial Biogeochemistry*, 2nd ed., Academic Press, London.

(13) Kern, M., Volz, J., and Simon, J. (2011) The oxidative and nitrosative stress defense network of *Wollinella succinogenes*: Cytochrome *c* nitrite reductase mediates the stress response to nitrite, nitric oxide, hydroxylamine and hydrogen peroxide. *Environ. Microbiol. 13*, 2478−2494.

(14) Tikhonova, T., Tikhonov, A., Trofimov, A., Polyakov, K., Boyko, K., Cherkashin, E., Rakitina, T., Sorokin, D., and Popov, V. (2012) Comparative structural and functional analysis of two octaheme nitrite reductases from closely related *Thioalkalovibrio* species. *FEBS J. 279*, 4052−4061.

(15) Mowat, C. G., and Chapman, S. J. (2005) Multi-heme cytochromes: New structures, new chemistry. *J. Chem. Soc., Dalton Trans. 21*, 3381−3389.

(16) Bewley, K. D., Ellis, K. E., Firer-Sherwood, M. A., and Elliott, S. J. (2013) Multi-heme proteins: Nature's electronic multi-purpose tool. *Biochim. Biophys. Acta 1827*, 938−948.

(17) Youngblut, M., Pauly, D. J., Stein, N., Walters, D., Conrad, J. A., Moran, G. R., Bennett, B., and Pacheco, A. A. (2014) *Shewanella oneidensis* cytochrome *c* nitrite reductase (ccNiR) does not disproportionate hydroxylamine to ammonia and nitrite, despite a strongly favorable driving force. *Biochemistry 53*, 2136−2144.

(18) Kostera, J., McGarry, J. M., and Pacheco, A. A. (2010) Enzymatic Interconversion of Ammonia and Nitrite: The Right Tool for the Job. *Biochemistry 49*, 8546−8553.

(19) Kostera, J., Youngblut, M. D., Slosarczyk, J. M., and Pacheco, A. A. (2008) Kinetic and product distribution analysis of NO reductase activity in *Nitrosomonas europaea* hydroxylamine oxidoreductase. *JBIC, J. Biol. Inorg. Chem. 13*, 1073−1083.

(20) Homer, R. F., and Tomlinson, T. E. (1960) The stereochemistry of the bridged quaternary salts of 2,2′-bipyridyl. *J. Chem. Soc.*, 2498−2503.

(21) Stein, N. (2014) Spectroscopic and electrochemical studies of *Shewanella oneidensis* cytochrome c nitrite reductase, and improving c-heme expression systems. Department of Chemistry and Biochemistry, University of Wisconsin—Milwaukee, Milwaukee, WI.

(22) Judd, E. T., Stein, N., Pacheco, A. A., and Elliott, S. J. (2014) Hydrogen bonding networks tune proton-coupled redox steps during the enzymatic six-electron conversion of nitrite to ammonia. *Biochemistry 53*, 5638−5646.

(23) Heineman, W. R., Norris, B. J., and Goelz, J. F. (1975) Measurement of enzyme $E^{0'}$ values by optically transparent thin layer electrochemical cells. *Anal. Chem. 47*, 79−84.

(24) Pilkington, M. B. G., Coles, B. A., and Compton, R. G. (1989) Construction of an optically transparent thin layer electrode cell for use with oxygen-sensitive species in aqueous and non-aqueous solvents. *Anal. Chem. 61*, 1787−1789.

DOI: 10.1021/acs.biochem.5b00330
Biochemistry 2015, 54, 3749−3758

(25) Watanabe, T., and Honda, K. (1982) Measurement of the extinction coefficient of the methyl viologen cation radical and the efficiency of its formation by semiconductor photocatalysis. *J. Phys. Chem. 86*, 2617−2619.
(26) Press, W. H., Teukolsky, S. A., Vetterling, W. T., and Flannery, B. P. (2007) *Numerical Recipes: The art of scientific computing*, 3rd ed., pp 65−75, Cambridge University Press, New York.
(27) Henry, E. R., and Hofrichter, J. (1992) Singular Value Decomposition: Application to Analysis of Experimental Data. In *Methods in Enzymology* (Brand, L., and Johnson, M. L., Eds.) pp 129−192, Academic Press, San Diego.
(28) Hagen, W. R. (1992) EPR spectroscopy of iron-sulfur proteins. *Adv. Inorg. Chem. 38*, 165−222.
(29) Walker, F. A. (1999) Magnetic spectroscopic (EPR, ESEEM, Mossbauer, MCD and NMR) studies of low-spin ferriheme centers nad their corresponding heme proteins. *Coord. Chem. Rev. 186*, 471−534.
(30) Spinner, F., Cheesman, M. R., Thomson, A. J., Kaysser, T., Gennis, R. B., Peng, Q., and Peterson, J. (1995) The haem b_{558} component of the cytochrome *bd* quinol oxidase complex from *Escherichia coli* has histidine-methionine axial ligation. *Biochem. J. 308*, 641−644.
(31) Walker, F. A., Huynh, B. H., Scheidt, W. R., and Osvath, S. R. (1986) Models of the cytochromes *b*. Effect of axial ligand plane orientation on the EPR and Mossbauer spectra of low-spin ferrihemes. *J. Am. Chem. Soc. 108*, 5288−5297.
(32) Shokhirev, N. V., and Walker, F. A. (1998) Co- and counterrotation of magnetic axes and axial ligands in low-spin ferriheme systems. *J. Am. Chem. Soc. 120*, 981−990.
(33) Li, J., Noll, B. C., Schultz, C. E., and Scheidt, W. R. (2007) New insights on the electronic and molecular structure of cyanide-ligated iron(III) porphyrinates. *Inorg. Chem. 46*, 2286−2298.
(34) Hendrich, M. P., Petasis, D., Arciero, D. M., and Hooper, A. B. (2001) Correlations of structure and electronic properties from EPR spectroscopy of hydroxylamine oxidoreductase. *J. Am. Chem. Soc. 123*, 2997−3005.
(35) Marritt, S. J., Kemp, G. L., Xiaoe, L., Durrant, J. R., Cheesman, M. R., and Butt, J. N. (2008) Spectroelectrochemical characterization of a pentaheme cytochrome in solution and as electrocatalytically active films on nanocrystalline metal-oxide electrodes. *J. Am. Chem. Soc. 130*, 8588−8589.
(36) Kurnikov, I. V., Ratner, M. A., and Pacheco, A. A. (2005) Redox equilibria in hydroxylamine oxidoreductase. Electrostatic control of electron redistribution in multielectron oxidative processes. *Biochemistry 44*, 1856−1863.
(37) Rivera, M., Seetharaman, R., Girdhar, D., Wirtz, M., Zhang, X. J., Wang, X. Q., and White, S. (1998) The reduction potential of cytochrome b_5 is modulated by its exposed heme edge. *Biochemistry 37*, 1485−1494.
(38) Wirtz, M., Oganesyan, V., Zhang, X. J., Studer, J., and Rivera, M. (2000) Modulation of redox potential in electron transfer proteins: Effects of complex formation on the active site microenvironment of cytochrome b_5. *Faraday Discuss.*, 221−234.
(39) Collins, M. J., Arciero, D. M., and Hooper, A. B. (1993) Optical Spectropotentiometric Resolution of the Hemes of Hydroxylamine Oxidoreductase: Heme Quantitation and pH-Dependence of E_m. *J. Biol. Chem. 268*, 14655−14662.
(40) Igarashi, N., Moriyama, H., Fujiwara, T., Fukumori, Y., and Tanaka, N. (1997) The 2.8 angstrom structure of hydroxylamine oxidoreductase from a nitrifying chemoautotrophic bacterium, *Nitrosomonas europaea*. *Nat. Struct. Biol. 4*, 276−284.

DOI: 10.1021/acs.biochem.5b00330
Biochemistry 2015, 54, 3749−3758